Effects of crystalline microstructure on epitaxial growth

Jacques G. Amar and Fereydoon Family
Department of Physics, Emory University, Atlanta, Georgia 30322
(Received 29 March 1996; revised manuscript received 20 August 1996)

The results of kinetic Monte Carlo simulations of epitaxial growth on fcc(100) and bcc(100) surfaces in which the correct crystal geometry is taken into account are reported. The existence of downward funneling to fourfold hollow sites leads to a downward current for large angles and to angle selection as observed in a variety of experiments. We have used our model to simulate Fe/Fe(100) deposition at room temperature and have compared our results with recent experiments. Excellent agreement is found for the selected angle, mound coarsening exponent n, and kinetic roughening exponent β as well as for the mound morphology. A theoretical analysis also leads to an accurate prediction of the observed mound angle for Fe/Fe(100) deposition at room temperature. The general dependence of the surface skewness, mound angle, and coarsening kinetics on temperature, deposition rate, and strength of the step barrier to interlayer diffusion is also studied and compared with recent experiments. While for a moderate step barrier we find an effective coarsening exponent $n \simeq 0.16-0.25$, for the case of a very large step barrier we find $n \simeq \frac{1}{3}$, which is significantly larger than found in previous models but in agreement with recent experiments on Rh/Rh(111). [S0163-1829(96)05544-0]

I. INTRODUCTION

Molecular-beam epitaxy (MBE) is one of the most effective techniques for growing high-purity materials including a variety of semiconductors and magnetic materials for applications in electronic and optoelectronic devices.[1] In this method a constant flux of atoms impinge under ultrahigh vacuum conditions on a substrate held at a fixed temperature to grow a high-quality crystalline material. The long-standing scientific challenge in this area is to model epitaxial growth conditions and understand what are the fundamental processes that control the evolution of epitaxial structure and morphology.

One way to develop a truly atomistic model of MBE growth is to include all the potentials between the particles and solve the dynamical equations for the motion of every atom in the system. A good approximation to this approach is used in molecular-dynamics simulations, which have provided a great deal of information about microscopic processes. However, due to limitations in computational power, the time scales and system sizes that can be realistically simulated are too limited to allow study of systems at the time scales and length scales of experimental interest. For this reason, much of the interest in modeling epitaxial growth has concentrated on the development of kinetic Monte Carlo simulation models, which take into account only processes that are considered to be crucial for understanding and simulating long-time and large-scale properties of the system.

One of the goals of developing growth models is to simulate how the morphology evolves with time. However, with the rapid progress and improvements in experimental techniques that have provided detailed atomistic information about MBE growth, a number of unexpected features of surface evolution and morphology have been observed. In particular, a number of recent experiments[2–9] have observed the existence of mounds or facets with a typical length scale and selected angle that coarsen with time. While the existence of an instability due to the Erhlich-Schwoebel barrier to interlayer diffusion[10] has been predicted by Villain[11] and subsequently verified in discrete and continuum models,[4,12–14] the detailed coarsening and roughening behavior is still not completely understood. Furthermore, the origin and value of the selected angle in various experiments is not well understood.

One of the fundamental problems with existing kinetic Monte Carlo models is the assumption that growth takes place on a simple-cubic lattice with the solid-on-solid (SOS) growth rule. In these models, while atoms may perform activated hopping in a direction parallel to the substrate, atoms that diffuse from the top of one column to the top of another column must perform ''infinite'' vertical diffusion in order to maintain the SOS condition. As has been pointed out,[15] this may lead to such anomalies as a ''grooved state'' with large ''cliffs'' and diverging slopes[12,16] as well as ''anomalous scaling.''[15,17] In the case of an instability due to a positive Ehrlich-Schwoebel barrier, it may also lead to dynamical behavior and morphology that does not agree with experiments.

In contrast, if the crystal geometry is correctly taken into account, then due to the epitaxial nature of the growth there exists a crucial dynamical process (sometimes called ''downward funneling'')[18] that initially must take place when an atom randomly lands on the surface. This is the process by which some of the initial energy of condensation of the deposited atom is dissipated as it moves and relaxes through a series of cascades until it reaches an epitaxial site on the surface. Such a microscopic process is not naturally built into the usual solid-on-solid models, but it fundamentally alters the growth and the morphology of the surface by limiting the steepest angles on the surface. From the point of view of recent continuum theories of epitaxial growth,[4,11,14,19] such cascade processes may be thought of as contributing to a downward current that overcomes the upward current due to the Ehrlich-Schwoebel barrier[10] and leads to a selected angle.

In this paper we present the results of kinetic Monte Carlo

 © 1996 The American Physical Society

simulations of epitaxial growth that take the crystal structure correctly into account. In particular, we present results obtained using our model to study multilayer growth in Fe/Fe(100) at room temperature. We find that the existence of the Ehrlich-Schwoebel barrier to interlayer diffusion leads to the formation and coarsening of mounds as observed in recent experiments.[2–9] In particular, we find good agreement with experimental results[6,20] for the value of the selected mound angle, mound coarsening dynamics, and surface roughening behavior.[21] We also present a theoretical analysis based on the crystal geometry and system parameters that leads to an accurate estimate of the experimental mound angle at room temperature.

In addition to these room-temperature results for Fe/Fe(100), we have also studied the dependence of the mound angle and coarsening dynamics on the strength of the interlayer diffusion barrier and on temperature. In particular, results are presented for both the case of a very small and a very large interlayer diffusion barrier, as well as for temperatures significantly lower and slightly higher than room temperature. We note that while Fe(100) corresponds to a bcc(100) surface, the crystal symmetry of the fcc(100) surface is the same and therefore our model and results may also be applicable to describe fcc(100) growth. Accordingly, we also present a comparison between our results and recent experiments on mound formation and coarsening in Cu/Cu(100) (Ref. 5) and Ag/Ag(100).[22] We also compare our results with those found for Rh/Rh(111),[9] although in this case the crystal symmetry is different. We note that elsewhere[23] we have presented a comparison between simulated diffraction profiles obtained using our model and recent diffraction experiments for Fe/Fe(100) at room temperature.[6,20]

The paper is organized as follows. In Sec. II we present the details of our model as well as the parameters chosen to mimic Fe/Fe(100) epitaxy. In Sec. III we present our theoretical and simulation results. Finally, in Sec. IV we present a discussion of results and conclusions.

II. MODEL AND SIMULATIONS

In our model atoms are randomly deposited at a rate $F/2$ per lattice site per unit time (corresponding to F layers per unit time) onto a square lattice [see Fig. 1(a)] corresponding to the bcc(100) substrate. As already noted, since the crystal symmetry is the same for an fcc(100) substrate, Fig. 1 also corresponds to growth on a fcc(100) substrate such as Ag(100) or Cu(100). However, in this case the arrows in Fig. 1 correspond to the (011) and (011) directions, respectively, rather than the (001) and (010) directions.[24]

Due to the epitaxial nature of the growth, deposited atoms are incorporated into the system only at the fourfold hollow sites formed by the four nearest-neighbor atoms in the layer below. This implies that if the deposited atom lands directly on a fourfold hollow site [see Fig. 1(c)] then it becomes part of the surface. However, if one or more of the nearest-neighbor sites has height lower than that of the deposition site before deposition [Fig. 1(b)] so that the deposition site does not correspond to a fourfold hollow site, then the freshly deposited atom ''cascades'' randomly to one of these lower sites. This process is then repeated at the new site,

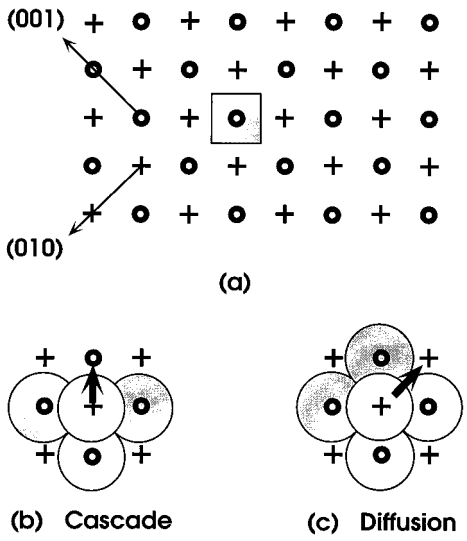

FIG. 1. (a) Square lattice of deposition sites used in simulation of growth on a bcc(100) substrate. Initially, the sites labeled+ correspond to the top layer and form fourfold hollows, while the sites labeled with open circles are one layer below. The shaded square shows the catchment area for the deposition site in the center. (b) Cascade to an epitaxial site after deposition. (c) Diffusion across a bridge site to a next-nearest-neighbor site.

until a fourfold hollow is found, although typically no more than two cascade processes ever takes place. The existence of such ''cascade'' processes corresponds to the fact that initially deposited atoms will dissipate some of their energy of condensation and to the fact that at not too low temperatures, growth will proceed epitaxially, i.e., atoms will relax to fourfold hollow sites shortly after deposition.

Once atoms have reached the nearest fourfold hollow site, they are then allowed to diffuse along with all the other atoms on the surface. As shown in Fig. 1(c), atoms are allowed to diffuse along the next-nearest-neighbor direction across the bridge sites of the fourfold hollow. The probability of diffusion is determined by the number of next-nearest-neighbor (in-plane) bonds of each atom as well as by whether or not the atoms jump down a step. In particular, the diffusion (hopping) rate for atoms on a flat surface with no next-nearest-neighbor bonds is given by $D=D_0e^{-E_a/k_BT}$, where E_a is the activation energy for monomer diffusion, while the rate for atoms with n in-plane bonds is given by $D_n=De^{-E_n/k_BT}$. For monomers that diffuse to a site that is not a fourfold hollow site (which would correspond to going down a step) an extra step-barrier energy [the Ehrlich-Schwoebel barrier E_B (Ref. 10)] is assumed so that the diffusion rate is given by $D_{\text{step}}=De^{-E_B/k_BT}$. In order to maintain epitaxy, such an adatom then cascades to the nearest fourfold hollow site at the bottom of the step. We note that, depending on the situation, such a process may actually occur preferentially via an ''adatom exchange'' [25,26] so that rather than hopping over the edge and cascading to the nearest fourfold site the adatom ''pushes'' the adatom below it to the adjoining fourfold site on the terrace below and replaces the position of the atom it has pushed out. While the identity of the two atoms is reversed in this case, from the point of

view of our Monte Carlo simulation the result is the same and therefore we do not distinguish between the case of a step barrier for adatom exchange or adatom hopping but instead lump both processes into one overall step barrier. We note that while our simulations may be able to provide an estimate of the overall barrier, a detailed microscopic calculation such as in Ref. 26 will be needed to determine the dominant mechanism.

In order to take into account cluster relaxation, the possibility of a different rate of diffusion for atoms with one bond along the edge of a cluster was also included in our simulations by assuming that the rate of edge-diffusion of one-bonded atoms is given by $D_e = De^{-E_e/k_BT}$. Finally, we have also included in our simulations the possibility of an additional process, ''transient kinetics'' at a step edge, according to which freshly deposited atoms at a step edge without any lateral bonds may immediately hop (with probability $\frac{1}{4}$ per step-edge) to the nearest fourfold hollow site below. This is equivalent to the ''knockout'' process at step edges observed in field ion microscopy of Rh deposited on Ir/Ir(111) clusters.[25] More specifically, in the case of transient kinetics one of the four next-nearest-neighbor directions of a freshly deposited atom at a step edge with no next-nearest-neighbor bonds is randomly selected. If the direction selected corresponds to a step edge then the hop is accepted; otherwise no hop is made.[27] Simulations were carried out both with and without transient kinetics at a step edge. However, the qualitative features of our results are independent of whether or not transient kinetics was included.

III. RESULTS

In order to compare with recent experiments on Fe/Fe(100) deposition at room temperature we have carried out simulations using parameters appropriate for this case. In particular, the experimental estimate $E_a \simeq 0.45$ eV (Ref. 28) was used, while the prefactor D_0 ($D_0 = 1.8 \times 10^{11}$ sec^{-1}) was obtained by matching the island density in our simulations with experiments at $\theta = 0.07$ ML.[28] We have also taken $E_1 = 0.6$ eV (using an estimate[29,30] based on the submonolayer island density at high temperature). This leads to negligible one-bond detachment at room temperature and is consistent with previous experimental evidence indicating that the critical island size for Fe/Fe(100) at room temperature is equal to 1.[28] In order to match the approximately square but slightly irregular submonolayer island morphology observed at room temperature,[28] simulations were carried out for values of the edge-diffusion barrier in the range $E_e = 0.1$–0.125 eV. The energy barrier E_B was then estimated as in Ref. 30 by matching our simulation results for the root-mean-square surface width to the experimentally observed values at room temperature[28,32] in the first few layers of growth (see Fig. 4). For $E_e = 0.1$ eV we obtained $E_B \simeq 0.055$ eV without transient kinetics and $E_B \simeq 0.06$ eV with transient kinetics, while for $E_e = 0.125$ eV we obtained $E_B \simeq 0.065$ eV without transient kinetics and $E_B \simeq 0.07$ eV with transient kinetics. We note that these values are close to those previously obtained[30] using a simple-cubic lattice model to study the first few layers of growth and are also consistent with estimates made using a rate-equation approach to estimate the coverage at which second layer nucleation takes place.[31,33] A similar but somewhat lower estimate of the step barrier assuming instantaneous restructuring of island edges has been made in Ref. 34.

A. Quantities measured

In order to quantitatively characterize the surface morphology we have calculated a variety of quantities as a function of the average layer height $\langle h \rangle$, where $h(\mathbf{r})$ is the height in layers at site $\mathbf{r}$. These include the circularly averaged height-height correlation function $G(r) = \langle \tilde{h}(\mathbf{0}) \tilde{h}(\mathbf{r}) \rangle_C$, where $\tilde{h}(\mathbf{r}) = h(\mathbf{r}) - \langle h \rangle$, as well as the root-mean-square surface fluctuation or surface width $w = [G(0)]^{1/2}$. As in the experimental analysis used in Ref. 6, the average mound size or feature separation ($2r_c$) was estimated from $G(r)$, where r_c is the position of the first zero crossing of $G(r)$. The ratio w/r_c, which is proportional to the tangent of the average mound angle, was also calculated in order to compare with the experimental results of Ref. 6. From the dependence of surface width and feature separation on film thickness $\langle h \rangle$, the kinetic roughening or growth exponent β ($w \sim \langle h \rangle^{\beta}$) and coarsening exponent $n = 1/z$ ($r_c \sim \langle h \rangle^n$) were obtained. In order to study the existence of asymmetry in the surface due to the crystal structure and/or the step barrier, the third moment of the height fluctuations around the average height $\kappa_3 = \langle (h - \langle h \rangle)^3 \rangle$ was also measured and used to calculate the scaled skewness $S_3 = \kappa_3 / w^3$.

In order to compare with recent experiments in which the evolution of the surface morphology was studied, our simulations were carried out using two different deposition rates: a ''slow'' deposition rate ($F = 0.0257$ ML/sec), close to that used in the room-temperature high-resolution low-energy electron diffraction experiments of Ref. 20, and a ''fast'' deposition rate ($F = 0.51$ ML/sec), corresponding to the deposition rate used in a more recent scanning tunneling microscopy and reflection high-energy electron diffraction (RHEED) study.[6]

B. Mound morphology and coarsening behavior

Figure 2 shows gray-scale contour plots of the surface obtained from simulations at room temperature after deposition of 10 and 100 ML at both the fast and slow deposition rates. In both cases mound structures are observed that grow and coarsen with time.[4,6] However, due to the larger diffusion length in the case of slow deposition, in this case the mounds are somewhat larger than for fast deposition. A comparison of Fig. 2(c) with the corresponding experimental contour plot in Ref. 6 indicates that as in the experiment, the mounds are slightly irregular. We also note that approximately the same number of exposed surface layers are observed in our simulations as in the experiments.

Figure 3 shows the corresponding mound angle ratio w/r_c as a function of film thickness for both fast and slow deposition rates. Beyond the first 10–20 layers, the mound angle is essentially constant, although the mound angle ratio appears to saturate much more quickly for the case of fast deposition. The calculated value for w/r_c for the case of fast deposition (0.06–0.07) is very close to the corresponding experimental value $w/r_c = 0.06$–0.08,[6] while for the case of slow deposition the value (0.08–0.09) is slightly higher. The

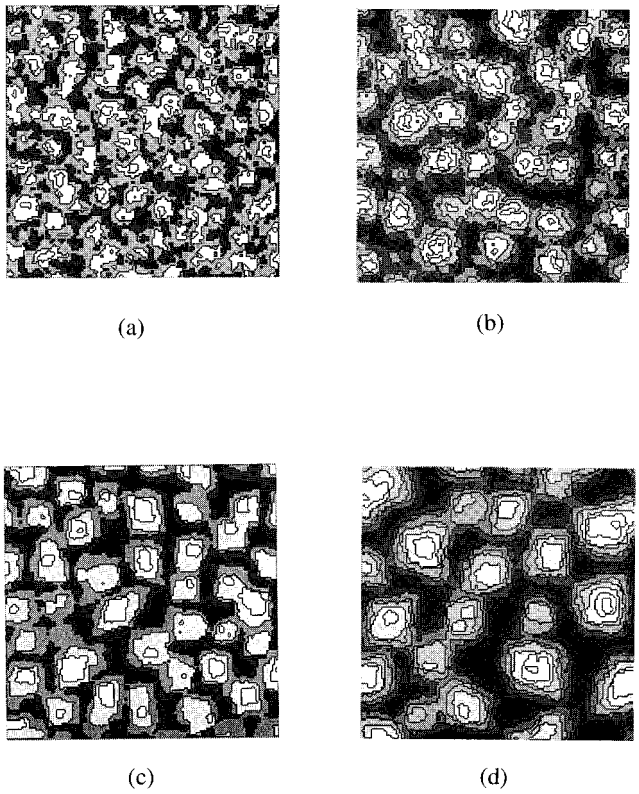

FIG. 2. Gray-scale images of a 37×37 nm^2 portion of surface obtained from simulations of Fe/Fe(100) deposition at $T=20$ °C. Lighter shades correspond to larger heights. The images have been rotated by 45° from Fig. 1 so that the edges are along the (001) and (010) directions. (a) Fast deposition rate, 10 ML; (b) fast deposition rate, 100 ML; (c) slow deposition rate, 10 ML; (d) slow deposition rate, 100 ML.

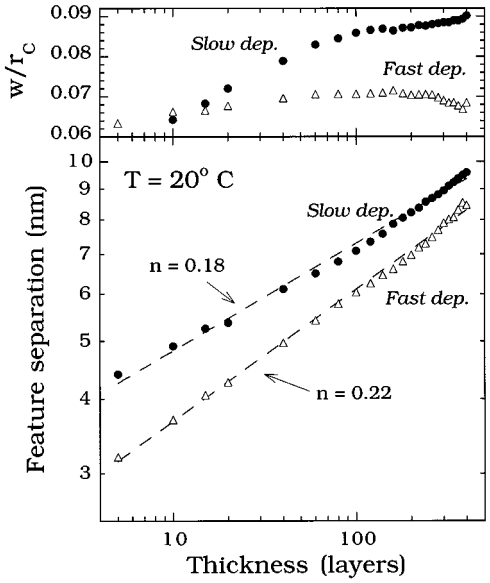

FIG. 3. Calculated feature separation ($2r_c$) and mound angle ratio w/r_c versus film thickness at $T=20$ °C for slow and fast deposition rates.

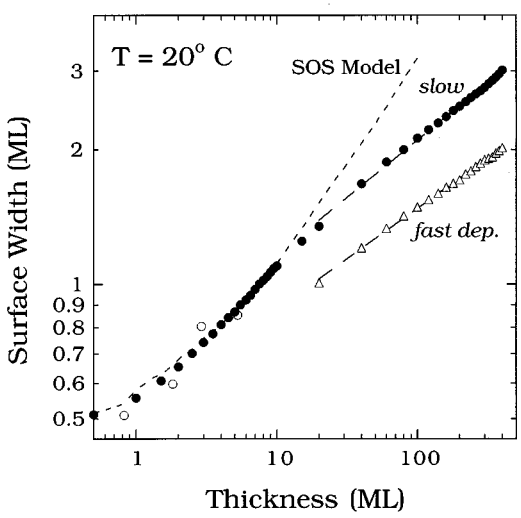

FIG. 4. Surface width w for bcc growth model at $T=20$ °C (slow and fast deposition) as well as corresponding results for simple-cubic SOS model (slow deposition). Power-law fits to late-time data (dashed lines) at $T=20$ °C give exponents $\beta=0.45\pm0.01$ (SOS model), $\beta=0.24\pm0.01$ (bcc model, slow deposition), and $\beta=0.22\pm0.02$ (bcc model, fast deposition). Open circles are experimental results (Ref. 28).

relatively weak dependence of w/r_c on deposition rate is consistent with the experimental results[6] in which slow deposition rates were used up to 20 ML, while fast deposition rates were used up to a thickness of several hundred layers.[32]

Also shown in Fig. 3 is the calculated feature separation in nanometers as a function of thickness. Power-law fits indicate the existence of a mound coarsening exponent n that is relatively insensitive to the deposition rate (0.18 ± 0.02 for slow deposition and 0.22 ± 0.02 for fast deposition). These values are consistent with but slightly above the experimental estimate $n\simeq0.16\pm0.04$.[6] We note, however, that fits to the later-time data give somewhat higher values ($n\simeq0.22$ and 0.25 for slow and fast deposition rates, respectively) close to the value $n\simeq\frac{1}{4}$ previously found in numerical simulations of a continuum model with angle selection.[14]

C. Roughening behavior

Figure 4 shows the corresponding simulation results for the surface width as a function of film thickness along with experimental data in the first few layers of growth.[28,32] The effective kinetic roughening exponent β, defined by $w\sim\langle h\rangle^{\beta}$, was found to be 0.24 ± 0.02 for slow deposition and 0.22 ± 0.02 for fast deposition, in good agreement with the experimental estimate[20] of $\beta=0.22\pm0.02$. The fact that the effective value of β is somewhat larger than the coarsening exponent over the same range of thickness appears to be due to the fact that the mound angle increases somewhat over this range. Also shown in Fig. 4 are results obtained for the corresponding SOS model on a simple-cubic lattice. As can be seen, at late times the surface roughness increases much more rapidly than in the experiment due to the lack of angle selection, leading to a significantly larger value for β ($\beta\simeq0.45$).

D. Measurement of surface current and selected angle

One explanation for the angle selection observed in our simulations is that the initial cascade upon deposition to a fourfold hollow site leads to a downward current that counterbalances the uphill current[4,11] due to the Ehrlich-Schwoebel step barrier E_B. For sufficiently large local slope m this leads to a stabilizing *negative* current. The value of the slope ($m=m_0$) for which the current is zero corresponds to the selected mound angle.[14] Accordingly, we have measured the surface current $J(m)$ in our simulations as a function of imposed slope m [with the surface tilted around the (001) axis] for both fast and slow deposition. As in Refs. 4 and 19, the scaled current J/F was measured by counting the number of hops made by an adatom in either the uphill or downhill direction (with uphill corresponding to a positive current and downhill to a negative current) and dividing by the number of particles deposited. For simplicity, the initial surface consisted of a regular array of straight steps with equal terrace widths, while the current was measured over the first 0.1 ML deposited.

Figure 5(a) shows our results for the case of fast deposition corresponding to the experiments in Ref. 6. As can be seen, the current is negative for sufficiently large slope both with and without transient kinetics. The range of values of m_0 obtained in our simulations (0.20–0.25) is in very good agreement with the experimental result[6] ($\theta=13°\pm3°$, $m=0.18$–0.29) for Fe/Fe(100) at room temperature as well as with estimates of the mound angle obtained from pictures such as those in Fig. 2. We note that for a bcc(100) surface this corresponds to a selected mound angle that is intermediate between that for a (103) facet and a (105) facet, while for growth on the equivalent fcc(100) surface, this would correspond to a mound slope that is intermediate between that for a (113) facet and a (115) facet.

Similar results are shown in Fig. 5(b) for the case of slow deposition. For small slopes the current is significantly larger than for fast deposition due to the increased diffusion length. However, for large slopes (e.g., small average terrace size) close to the selected angle the current is approximately the same for both cases. Accordingly, the value of the selected angle does not appear to depend strongly on deposition rate.

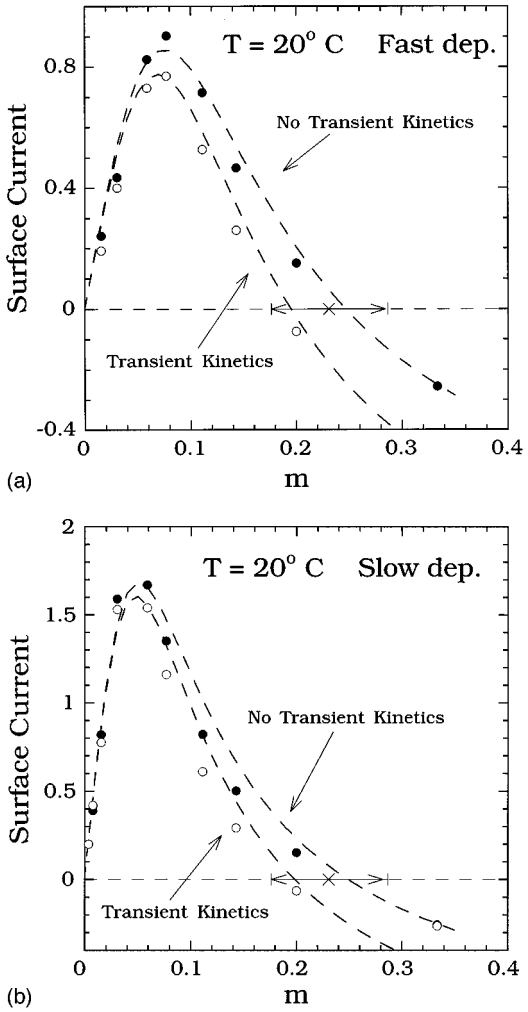

FIG. 5. Surface current $J/2F$ at room temperature as a function of imposed slope m both with (open circles) and without (filled circles) transient kinetics at step edges. Cross with arrows indicates experimental estimate (Ref. 6) of the mound angle for room-temperature Fe/Fe(100) deposition. Dashed lines are theoretical fits of the form of Eq. (6). (a) Fast deposition and (b) slow deposition.

E. Theoretical estimate of surface current and selected angle

The surface current $J(m)$ and selected angle may also be directly estimated from an analysis of the upward and downward currents that takes into account the crystal geometry. For simplicity, we consider a surface with slope m tilted around the [001] direction (see Fig. 1) consisting of a periodic array of terraces of width $l_t=1/m$ (in units of $\frac{1}{2}$ the next-nearest-neighbor distance) separated by straight steps running along the [001] direction [see Fig. 6(a)]. Assuming that the step barrier is perfectly reflecting (which is a reasonable approximation at room temperature), then the only contribution to the downward current comes from deposition at steps. As shown in Fig. 6(a), the downhill current for deposition at straight steps consists of two parts. The first part corresponds to deposition just below the top of a step and leads to a contribution to the current (again in units of $\frac{1}{2}$ the next-nearest-neighbor distance) of -1, since an adatom deposited at such a site will make one hop in the downward direction before bonding to the step. The second part corresponds to deposition at the top of a step and again leads to a contribution of -1, since an adatom deposited at such a site will cascade with probability $\frac{1}{2}$ via two downward hops to the bottom of the step. Summing and multiplying by the probability ($m=1/l_t$) that a deposited adatom will land on either of these sites, one obtains for the case without transient kinetics a negative (downhill) current that is proportional to the step density[35]

$$J_{\text{down}}(m)/F=-2|m|. \tag{1}$$

For the case of transient kinetics at step edges, there is an additional contribution due to atoms that land at a fourfold hollow site at the top of a step and then (with probability $\frac{1}{4}$) hop three units to the bottom of the step. This leads to a negative (downhill) current for this case given by

$$J^{\text{TK}}_{\text{down}}(m)/F=-7|m|/2. \tag{2}$$

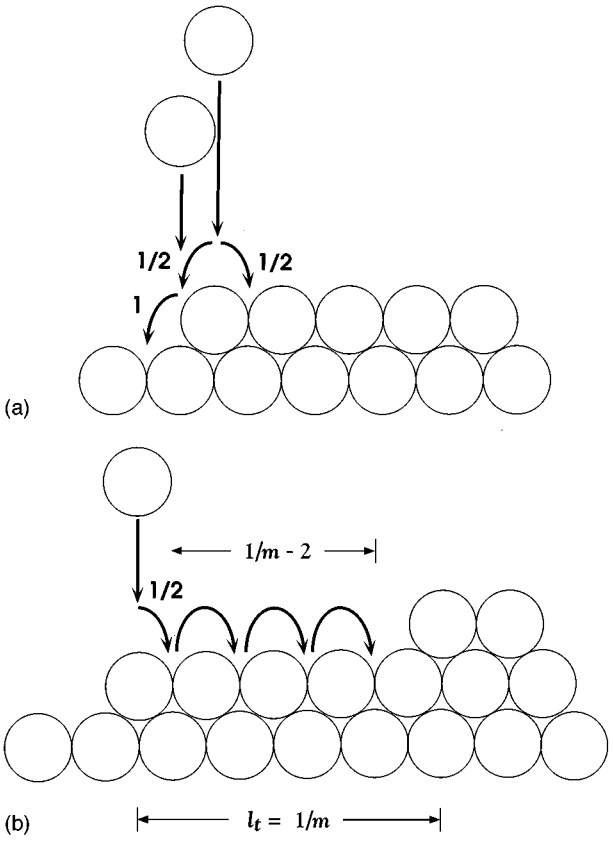

FIG. 6. Diagram showing contributions to surface current for an idealized (100) surface with straight step edges (side view) and slope m tilted around the (001) axis. (a) Downhill current at step edges and (b) uphill current.

The positive (uphill) contribution to the current may also be estimated by assuming that the step barrier is perfectly reflecting. This implies that for large enough slopes (e.g., terrace sizes smaller than a diffusion length σ) all atoms that land at the top of a step reach the nearest ascending step without attaching to or forming an island[4] and contribute a term equal to m times the distance to the nearest up step. In addition, atoms that land on the top edge of a step [see Fig. 6(b)] will cascade with probability $\frac{1}{2}$ to the terrace above and diffuse to the nearest up step. This leads to the sum $\tilde{J}_{\rm up}/F = m[1+2+3+\cdots+(1/m-3)]+(m/2)(1/m-2)$, so that for the case without transient kinetics at a step edge one has

$$\tilde{J}_{\rm up}/F = (1-2|m|)^2/2|m|. \tag{3}$$

Taking into account the additional downward current for the case of transient kinetics, we obtain for this case

$$\tilde{J}^{\rm TK}_{\rm up}/F = (1-13|m|/4)(1-4|m|)/2|m|+9/8-3|m|. \tag{4}$$

The selected mound angle may now be obtained by equating the magnitudes of the uphill and downhill currents. For the case without transient kinetics this leads using (1) and (3) to the estimate $m_0 \simeq 0.25$ or $\theta \simeq 14°$, which is in good agreement with experiment and with our simulations [see Fig. 5(a)]. For the case of transient kinetics we obtain $m_0 = 0.2$ or $\theta \simeq 11°$, again in reasonable agreement with our simulations and experiment.

We note that for small angles for which the terrace width is of the order of or larger than the diffusion length σ, the estimates (3) and (4) for the uphill current are incorrect. In particular, for very small slopes and large terrace widths ($m \ll 1/\sigma$), one expects that the uphill current will be proportional to the probability (σm) that an adatom lands within a distance σ of an up step, multiplied by the average distance traveled,[4,19] e.g., $J_{\rm up} \simeq \sigma^2 m$. In order to obtain an expression for $J_{\rm up}(m)$ that is correct for both large and small m, we therefore replace Eqs. (3) and (4) with the approximate form

$$J_{\rm up}(m) = \sigma^2 m/[1+\sigma^2 m/\tilde{J}_{\rm up}(m)], \tag{5}$$

which interpolates, between the $\sigma^2 m$ behavior for the uphill current for small m and our estimates (3) and (4) for large m, with $\tilde{J}_{\rm up}(m)$ given by (3) and (4). This leads to the following form for $J(m)$:

$$J(m) = \sigma^2 m/[1+\sigma^2 m/\tilde{J}_{\rm up}(m)] - J_{\rm down}(m), \tag{6}$$

where $\tilde{J}_{\rm up}(m)$ and $J_{\rm down}(m)$ are as given in Eqs. (1)–(4). Figures 5(a) and 5(b) show dashed-line fits using this form to our simulation results. As can be seen, there is very good quantitative agreement with the simulation results even for small slope m. As expected, the diffusion length σ is larger for the case of slow deposition ($\sigma \simeq 8$) than for fast deposition ($\sigma \simeq 5$). However, the measured current tends to be slightly below the theoretical fits due to the fact that the step barrier used in the simulations is not perfectly reflecting. We note that for $m \geq 0.1$ the difference between the surface current obtained using the interpolation form (5) for $J_{\rm up}(m)$ and that obtained using (3) and (4) directly is negligible.

F. Dependence of coarsening dynamics on step barrier E_B

In order to clarify the effect of the step barrier on mound formation and coarsening dynamics, we have also carried out simulations with different values of the step barrier. Simulations were carried out with no step barrier ($E_B = 0$) as well as with a very large, perfectly reflecting barrier ($E_B = 0.6$ eV). In order to compare with previous results, simulations were carried out at room temperature using the ''slow'' deposition rate ($F = 0.0257$ ML/sec) and both with and without transient kinetics at step edges.

1. No step barrier ($E_B = 0$)

Figure 7(a) shows a log-log plot of the surface width as a function of thickness for this case. As can be seen, the surface width exhibits significant although slightly damped oscillations indicative of layer-by-layer growth. A power-law fit to the later time behavior gives a very small growth exponent $\beta \simeq 0.08$, while the approximately linear behavior at late times on a semilog plot (not shown) indicates approximately logarithmic growth of the surface width. This behavior is consistent with the surface current $J(m)$ shown in the inset, which is negative due to the downward current at steps. This implies[11] a ''positive'' surface tension and logarithmic, Edwards-Wilkinson behavior[36] at long times.

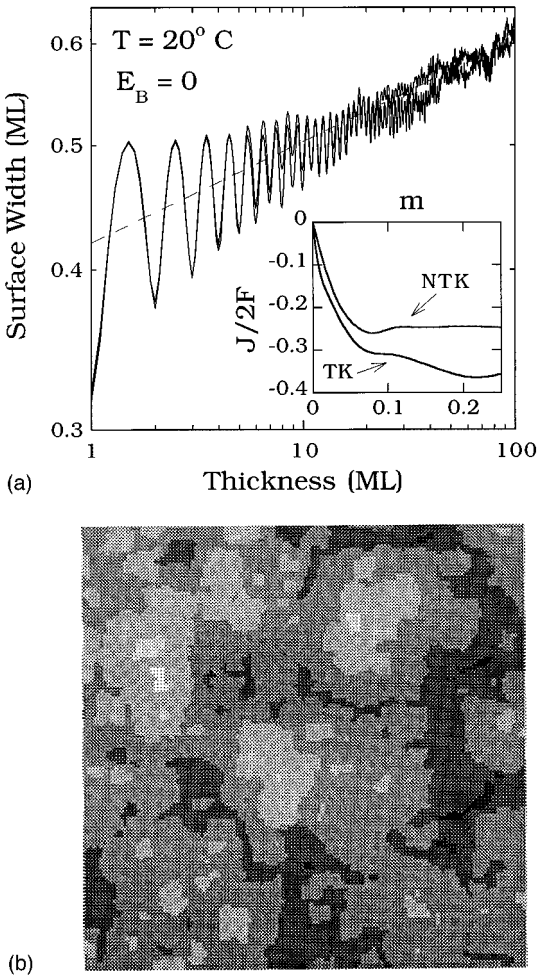

FIG. 7. (a) Surface width as a function of coverage at room temperature (slow deposition rate) for the case of no step barrier both with and without transient kinetics. The dashed-line fit has slope $\beta \simeq 0.08$. The inset shows the surface current as a function of slope m for both transient kinetics at a step edge (TK) and no transient kinetics (NTK). (b) 128×128 gray-scale plot of the surface at 100 ML. Lighter shades indicate higher levels. [Note that the surface has been rotated so that the sides are parallel to the (001) and (010) directions in Fig. 1.]

Figure 7(b) shows a gray-scale contour plot of the surface that indicates that after 100 layers have been deposited the surface is still quite flat and without mound formation. This is corroborated by the value of the mound angle ratio, which is found to be very small and decreases with increasing coverage (from $w/r_c = 0.02$ at 5 ML to $w/r_c = 0.005$ at 100 ML). However, power-law fits of the feature separation as a function of coverage (not shown) indicate a value of the coarsening exponent ($n \simeq 0.3$) that is somewhat less than expected for the case of Edwards-Wilkinson behavior ($n = 1/z = \frac{1}{2}$).

2. Large step barrier ($E_B = 0.6$ eV)

Figure 8 shows the mound angle ratio and feature separation as a function of coverage for the case of slow deposition at $T = 20$ °C with a very large (perfectly reflecting) step barrier ($E_B = 0.6$ eV) and both with and without transient kinetics at a step edge. In this case the mound angle ratio ($w/r_c \simeq 0.1$) is somewhat larger than for the case of a moderate barrier $E_B = 0.07$ eV (see Fig. 3) due to the increased uphill current. In addition, the mound angle ratio appears to saturate much more rapidly. Furthermore, the value of the late-time coarsening exponent ($n = 0.35 \pm 0.02$ with transient kinetics and $n = 0.32 \pm 0.01$ without transient kinetics) is significantly larger than obtained in our simulations in Sec. III A with $E_B = 0.07$ eV or obtained experimentally for Fe/Fe(100) deposition.[6] However, it is very close to the experimental value ($n = 0.33$) obtained for Rh/Rh(111) at 725 K.[9] Figure 9(a) shows a gray-scale plot of the surface for this case at 100 ML that shows the presence of many levels, while Fig. 9(b) shows the surface roughness as a function of coverage. Due to the rapid angle selection, the value of the roughening exponent ($\beta \simeq 0.30$ without transient kinetics and $\beta \simeq 0.32$ with transient kinetics) is close to the coarsening exponent.

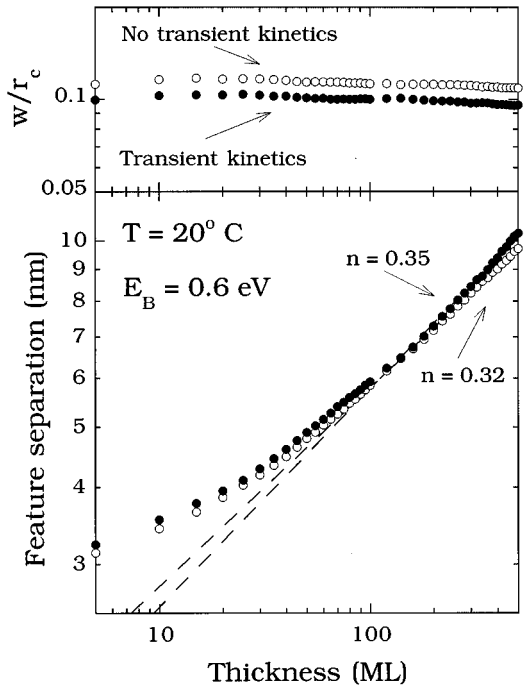

FIG. 8. Calculated feature separation ($2r_c$) and mound angle ratio w/r_c versus film thickness at $T = 20$ °C for the case of a very large step barrier ($E_B = 0.6$ eV) and slow deposition rate.

3. Surface skewness as a function of step barrier

Figure 10 shows our results for the surface skewness as a function of step barrier at room temperature. For the case of a large step barrier ($E_B = 0.6$ eV), the scaled skewness saturates rapidly to a constant value that is quite large ($\kappa_3/w^3 \simeq 0.15 \pm 0.03$). The rapid saturation of the scaled skewness is consistent with the rapid angle selection observed in Fig. 8. However, for the case of a moderate barrier ($E_B = 0.07$ eV) the skewness is actually negative at early times and is still increasing at 400 ML, although it appears to be approaching a finite positive value possibly close to that for a very large barrier at late times. As in Fig. 3 for the mound angle ratio, the approach of the skewness to saturation is more rapid for the case of fast deposition than for the case of slow deposition. For the case of no step barrier (not

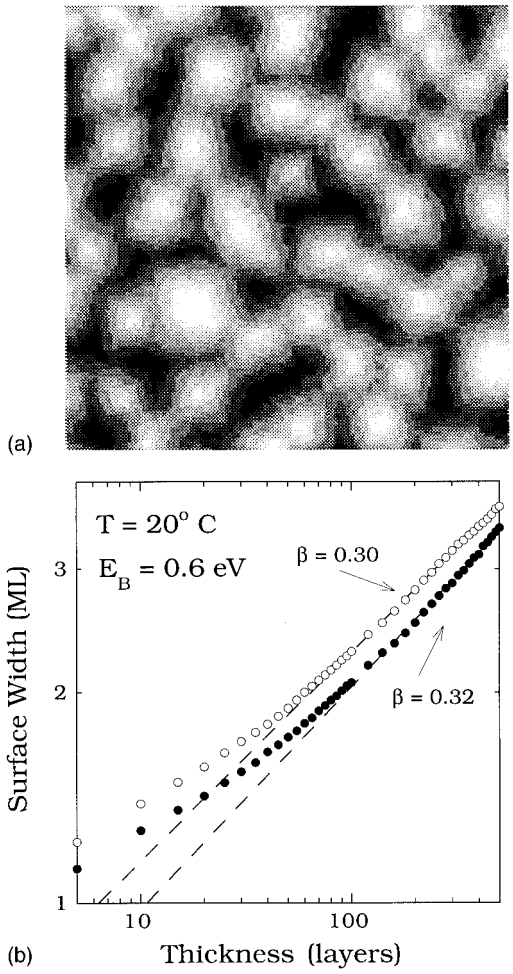

FIG. 9. (a) Gray-scale plot of surface at 100 ML for the case of a large step-barrier (E_B=0.6 eV) with slow deposition and no transient kinetics. (b) Surface width as a function of coverage for this case with (filled circles) and without (open circles) transient kinetics at step edges.

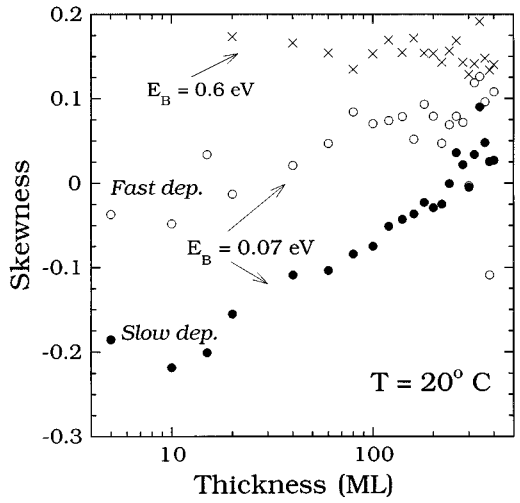

FIG. 10. Scaled surface skewness (κ_3/w^3) as a function of step barrier at T=20 °C.

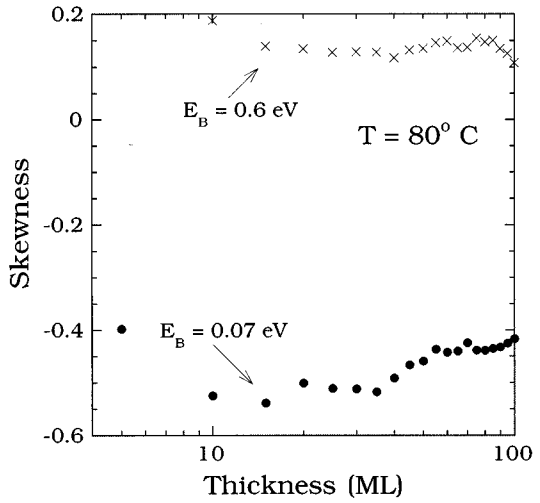

FIG. 11. Scaled surface skewness as a function of step barrier at T=80 °C.

shown) a constant but small negative skewness ($\kappa_3/w^3 \simeq -0.05 \pm 0.05$) is also observed. The negative skewness for the case of no step barrier appears to be due to the downward current, while the increasing positive skewness with increasing step barrier is due to the lack of inversion symmetry in the mounds, which tend to have relatively flat tops and narrower valleys.

Figure 11 shows similar results for the surface skewness at T=80 °C. Somewhat surprisingly, for the case of a moderate step barrier (E_B=0.07 eV), the scaled skewness starts out quite negative ($\kappa_3/w^3 \simeq -0.5$), although it again appears to be approaching a positive value. The slow approach of the skewness to saturation at T=80 °C is consistent with the relatively slow angle selection observed at this temperature for a moderate step barrier (see Sec. III G 2 below). On the other hand, for a very large step barrier (E_B=0.6 eV) we find rapid saturation of the skewness with a large positive value ($\kappa_3/w^3 = 0.13 \pm 0.03$) close to that found at room temperature.

G. Dependence of coarsening dynamics on temperature

In order to understand the temperature dependence of mound formation and kinetics we have also carried out simulations at very low temperature (T=0 K) as well as at temperatures slightly above and below room temperature.

1. Deposition at low temperature (T=0)

Figure 12(a) shows the surface width as a function of thickness for this case both with and without transient kinetics. The weak oscillations in the first few layers indicate partial layer-by-layer growth in agreement with the experimental observation of RHEED oscillations in low-temperature deposition on metal (100) surfaces.[37,38]

As shown by the gray-scale plot in Fig. 12(b), at 100 ML the surface is still relatively smooth, although the islands have a fairly irregular structure with small microfacets. Interestingly the surface width is only slightly higher than for the case of deposition at room temperature without a step barrier [see Fig. 7(a)], although the surface morphology is completely different. Due to the lack of diffusion

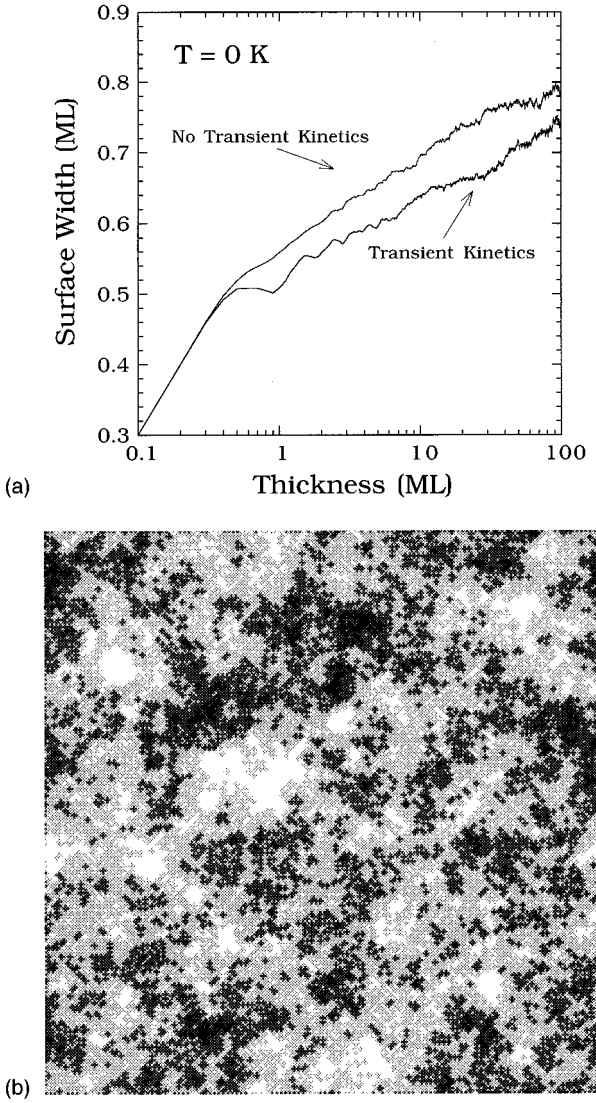

FIG. 12. (a) Surface width as a function of coverage at $T=0$ K. (b) Gray-scale plot of surface after deposition of 100 ML at $T=0$ K.

at low temperature there is no uphill current so the step barrier becomes ineffective. However, there is still a downhill current due to the cascade process to fourfold hollow sites. This leads to the approximate logarithmic, Edwards-Wilkinson-like[36] growth of the surface width at large coverage, shown in Fig. 12(a). We note that this behavior has also previously been observed[18] in models of random deposition at fourfold hollow sites with ''downward funneling.'' Measurement of the mound angle ratio w/r_c also indicates that there is no mound formation while fits to the behavior of r_c (which now corresponds to the correlation length rather than to the typical mound size) for the case without transient kinetics indicate that $n\simeq 0.5$, as expected for the case of Edwards-Wilkinson behavior.

2. Deposition above and below room temperature

In order to compare with our room-temperature results, we have also carried out simulations at temperatures somewhat below and above room temperature (with a moderate step barrier $E_B=0.07$ eV), as shown in Figs. 13 and 14. At

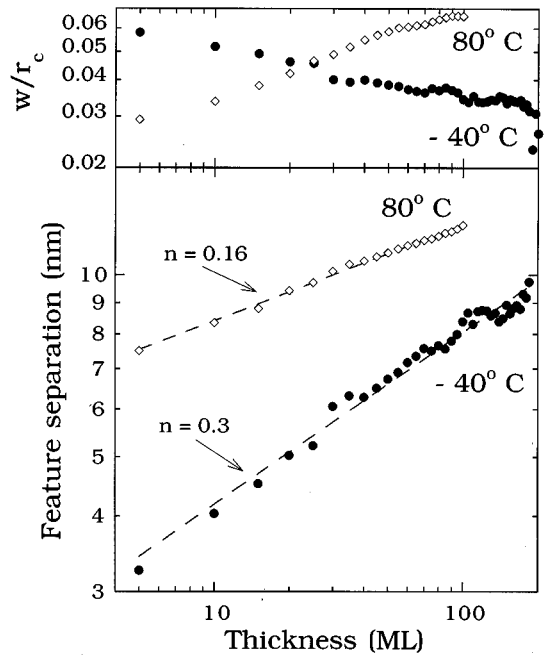

FIG. 13. Calculated feature separation ($2r_c$) and mound angle ratio w/r_c versus film thickness at $T=-40$ °C and 80 °C for the case of a moderate step barrier ($E_B=0.07$ eV) and slow deposition rate.

$T=-40$ °C the results are very similar to those obtained at zero temperature. In particular, due to the decreased diffusion length there is a significant reduction in the mound angle with increasing coverage as well as in the effective growth exponent ($\beta\simeq 0.13$), reflecting a possible crossover to Edwards-Wilkinson-like behavior.[36] Similarly, the effective coarsening exponent is significantly increased ($n\simeq 0.3$).

On the other hand, increasing the temperature from $T=20$ °C to 80 °C leads to a large increase in the effective roughening exponent in the first 100 layers ($\beta\simeq 0.45$), while

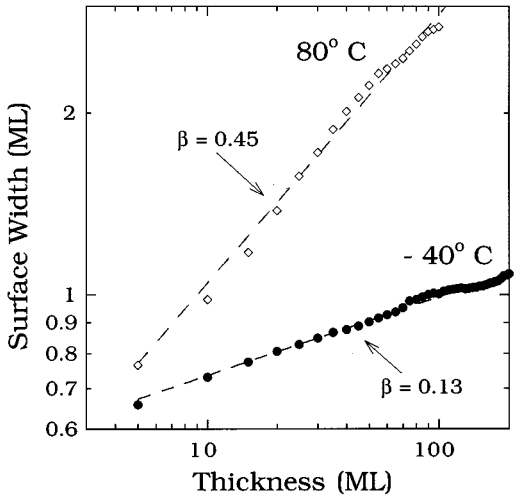

FIG. 14. Surface width as a function of coverage at $T=-40$ °C and 80 °C for the case of a moderate step barrier ($E_B=0.07$ eV) and slow deposition rate.

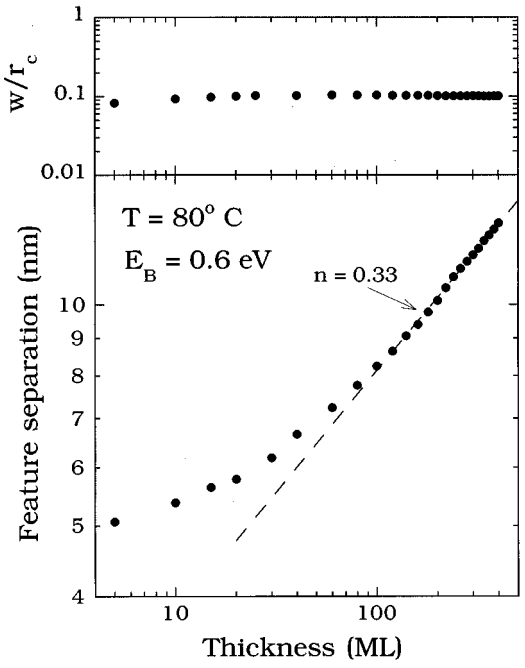

FIG. 15. Calculated feature separation ($2r_c$) and mound angle ratio w/r_c versus film thickness at $T=80$ °C for the case of a very large step barrier ($E_B=0.6$ eV) and slow deposition rate.

the coarsening exponent $n\simeq 0.16$ is relatively unchanged. The large increase in the effective roughening exponent appears to be due to the increase in the mound angle ratio w/r_c with coverage up 100 ML and the late saturation of the mound angle at higher temperature. Due to the decreased effectiveness of the step barrier, the mound angle ratio w/r_c is also some what lower than at room temperature. These results are qualitatively and quantitatively very similar to those obtained in recent experiments on low-temperature growth of Cu/Cu(100),[5] in which the roughness exponent was found to increase from $\beta=0.26$ at $T=160$ K to a value of $\beta=0.56$ at $T=200$ K, while the typical mound angle was found to decrease from (113) facets at the lower temperature to (115) facets at the higher temperature.

In order to clarify the behavior observed at room temperature for a very large step barrier (Sec. III F 2), we have also carried out simulations at $T=80$ °C with $E_B=0.6$ eV, as shown in Fig. 15. In this case, the effective coarsening exponent is again significantly larger than $\frac{1}{4}$ and is close to $\frac{1}{3}$ ($n\simeq 0.33$). Similarly, the mound angle ratio also saturates very quickly, indicating that there is very fast angle selection. We note that this is consistent with the fast saturation of the skewness for this case shown in Fig. 11. Accordingly, the effective roughening exponent ($\beta\simeq 0.32$, not shown) is close to the coarsening exponent.

IV. DISCUSSION

We have developed a model of epitaxial growth on bcc and fcc (100) surfaces that properly takes into account crystal geometry and eliminates the unphysical artifacts present in solid-on-solid models. This approach naturally leads to a negative downward current for large angles and to angle selection as observed in a variety of experiments. Applying our model to simulate Fe/Fe(100) deposition at room temperature, we have obtained good agreement with recent experiments for the selected mound angle, coarsening exponent n, and kinetic roughening exponent β. We have also presented a theoretical analysis of the surface current that leads to an accurate prediction of the experimental mound angle at room temperature.

As already noted, previous simulations using simple cubic lattice SOS models[4,12,16] do not lead to angle selection since processes that lead to a downward current such as a cascade to fourfold hollow sites are not naturally included in such models. Recently, however, attempts have been made to include additional mechanisms or parameters within the simple cubic lattice model framework in order to include such processes.[39,40] For example, in Ref. 39 an additional parameter corresponding to a reincorporation radius (such that freshly deposited atoms are immediately moved to the highest-coordination site within a certain radius of the deposition site) was introduced. In Ref. 40 ''knockout'' effects were simulated by allowing a fraction p of the deposited particles to immediately hop to a nearest-neighbor column of lower height, if one exists. In both cases, the addition of such processes leads to a selected mound angle. However, such an approach requires the addition of *ad hoc* parameters whose value cannot be directly related to physical processes. In contrast, in our approach the appropriate downward current and mound angle is obtained with no free parameters.

We now summarize our results in somewhat more detail. Our estimates for the effective coarsening exponent n for Fe/Fe(100) at room temperature (0.18 ± 0.02 for fast deposition and 0.22 ± 0.02 for slow deposition) are slightly higher, but still consistent with the measured value $n=0.16\pm 0.04$.[6] As already noted, fits to the later time data give somewhat higher estimates ($n\simeq 0.22\pm 0.01$ and 0.25 ± 0.01 for slow and fast deposition respectively). This indicates that the asymptotic value of the coarsening exponent is somewhat higher, and appears to be close to the value $\frac{1}{4}$ obtained numerically from the solution of a simple continuum equation with angle selection.[14] We note that since there is essentially no bond breaking at room temperature for the parameters used in our simulations, these results appear to contradict the assertion in Ref. 6 that $n\simeq\frac{1}{6}$ in the absence of detachment from islands. Rather, our results suggest that the value of the coarsening exponent obtained experimentally in Ref. 6 may be a crossover effect and the asymptotic value may be significantly larger. Such a crossover is consistent with the experimental data in Ref. 6.

We now summarize our results for the dependence of surface morphology and kinetics on the temperature and step barrier. For the limiting case of no step barrier, we found relatively persistent layer-by-layer growth at early times (no mound formation) and quasi-logarithmic Edwards-Wilkinson-type behavior at late times due to the negative current at step edges. Similarly for the case of very-low-temperature growth for which the step barrier becomes irrelevant, we again found relatively slow logarithmic growth of the surface width, although the surface morphology is quite different due to the very small diffusion length.

On the other hand, in simulations with a very large step barrier a significantly higher value ($n\simeq\frac{1}{3}$) for the coarsening exponent n was obtained. It should be emphasized that this

value is significantly higher than the value ($n \simeq \frac{1}{4}$) obtained from numerical integration of a simple continuum equation with angle selection[39] and is also higher than that previously obtained using SOS models.[40] The relatively fast saturation of the surface skewness for this case indicates that this may be the asymptotic value of the coarsening exponent. In contrast, the relatively slow saturation of the surface skewness for a moderate step barrier ($E_B = 0.07$ eV; see Fig. 10) suggests that for this case the exponent may not have reached its asymptotic value. One possibility is that the asymptotic coarsening exponent is $\frac{1}{3}$ for any reasonably large step barrier, with a relatively slow crossover for a moderately large step barrier. Another possibility is that there is a transition from asymptotic $n = \frac{1}{4}$ behavior to $n = \frac{1}{3}$ behavior with increasing step barrier due to a competition between different mechanisms for mound coarsening such as occurs in spinodal decomposition.[41] Further work will be needed to distinguish between these two possibilities. In any case, the relatively slow saturation of the surface skewness (compared to the saturation of the mound angle ratio w/r_c) suggests that the surface skewness may be a more sensitive test of whether or not one has reached the scaling regime than the mound angle ratio.

We note that the value obtained for the coarsening exponent in the case of a large step barrier is also close to the value ($n \simeq 0.33$) recently obtained in experiments on Rh/Rh(111) at 725 K. This appears to indicate that in the case of Rh/Rh(111) the step barrier is quite large, although it is also possible that the different (triangular) lattice structure of the (111) surface may play a role. Future work will be needed to determine if this is the case. We note that for the case of a very large step barrier the saturation of the mound angle was significantly faster than for a moderate step barrier so that the value of the roughening exponent ($\beta \simeq 0.30$ without transient kinetics at step edges) was close to that obtained for the coarsening exponent.

We have also presented results using our model for Fe/Fe(100) at a temperature slightly higher than room temperature. Surprisingly, we find that at $T = 80$ °C, while our estimate of the coarsening exponent ($n \simeq 0.16$) in the first 100 ML is close to that obtained at room temperature, the effective roughness exponent ($\beta \simeq 0.45$) is significantly larger due to the slow saturation of the mound angle. The slow saturation of the mound angle as well as the increased width appears to be due to the decreased effectiveness of the step barrier at higher temperature. These results may provide a qualitative explanation for the experimental results obtained for Cu/Cu(100) (Ref. 5) in which the roughness exponent was found to increase from $\beta = 0.26$ at $T = 160$ K to a value of $\beta = 0.56$ at $T = 200$ K, while the typical mound angle was found to decrease from (113) facets at the lower temperature to (115) facets at the higher temperature. We note that the values obtained for the roughening and coarsening exponent at $T = 80$ °C are also consistent with recent asymptotic predictions ($\beta = \frac{1}{2}$, $n = \frac{1}{6}$) obtained by Golubovic[42] from an analysis of an isotropic continuum equation with a higher-order $\nabla^6 h$ term replacing the usual equilibrium $\nabla^4 h$ term and with a slope instability but without angle selection. Similar behavior for the coarsening exponent n has also been observed in recent simulations of a SOS model with a moderately strong step barrier but without angle selection.[43] The difference between these results and those obtained with strong angle selection indicates that angle selection may also play an important role in determining the coarsening exponent.

Finally, we note that at high enough temperatures, one expects the roughness exponent and surface width for Fe/Fe(100) to decrease with temperature and layer-by-layer growth to set in due to the decreased effectiveness of the step barrier. This is clearly shown by the experimental results showing layer-by-layer growth at $T = 250$ °C in Ref. 28. Along with our low-temperature results, this implies reentrant behavior for the surface width as a function of temperature. However, at an intermediate temperature ($T = 130$ °C–180 °C) recent experiments on Fe/MgO(001) deposition[7] have led to pyramid formation in which [012] facets were observed. The existence of large regular mounds in this case is indicative of a relatively strong step barrier, while the value of the coarsening exponent ($n = \frac{1}{4}$) is consistent with our results for a moderately strong step barrier as well. It is not clear whether or not strain effects are important in this system, but in any case, further simulations will be needed to fully explain these results.

ACKNOWLEDGMENTS

This work was supported by National Science Foundation Grants Nos. DMR-9214308 and DMR-9520842 and by the Office of Naval Research. We would like to thank Joseph Stroscio for providing us with experimental data for Fe/Fe(100) in the first few layers of growth, Ted Einstein and Brad Orr for useful discussions, and David Akers for help with the visualization. Part of this work was carried out using the computational facilities of the Cherry L. Emerson Center for Scientific Computation at Emory University.

[1] See, for example, J. Y. Tsao, *Materials Fundamentals of Molecular Beam Epitaxy* (World Scientific, Singapore, 1993).

[2] G. W. Smith, A. J. Pidduck, C. R. Whitehouse, J. L. Glasper, and J. Spowart, J. Cryst. Growth **127**, 966 (1993).

[3] M. Albrecht, H. Fritzsche, and U. Gradmann, Surf. Sci. **294**, 1 (1993).

[4] M. D. Johnson, C. Orme, A. W. Hunt, D. Graff, J. Sudijono, L. M. Sander, and B. G. Orr, Phys. Rev. Lett. **72**, 116 (1994).

[5] H.-J. Ernst, F. Fabre, R. Folkerts, and J. Lapujoulade, Phys. Rev. Lett. **72**, 112 (1994).

[6] J. A. Stroscio, D. T. Pierce, M. Stiles, A. Zangwill, and L. M. Sander, Phys. Rev. Lett. **75**, 4246 (1995).

[7] K. Thürmer, R. Koch, M. Weber, and K. H. Rieder, Phys. Rev. Lett. **75**, 1767 (1995).

[8] J. E. Van Nostrand, S. Jay Chey, M.-A. Hasan, D. G. Cahill, and J. E. Greene, Phys. Rev. Lett. **74**, 1127 (1995).

[9] F. Tsui, J. Wellman, C. Uher, and R. Clarke, Phys. Rev. Lett. **76**, 3164 (1996).

[10] G. Ehrlich and F. Hudda, J. Chem. Phys. **44**, 1039 (1966); R. L. Schwoebel, J. Appl. Phys. **40**, 614 (1969).

[11] J. Villain, J. Phys. (France) I, **1**, 19 (1991).
[12] Z. Zhang, J. Detch, and H. Metiu, Phys. Rev. B **48**, 4972 (1993); I. Elkinani and J. Villain, J. Phys. (France) I **4**, 949 (1994); J. Krug and M. Schimschak, *ibid*. **5**, 1065 (1995); C. J. Lanczycki and S. Das Sarma, Phys. Rev. Lett. **76**, 780 (1996).
[13] A. W. Hunt, C. Orme, D. R. M. Williams, B. G. Orr, and L. M. Sander, Europhys. Lett. **27**, 611 (1994).
[14] M. Siegert and M. Plischke, Phys. Rev. Lett. **73**, 1517 (1994).
[15] J. G. Amar, P.-M. Lam, and F. Family, Phys. Rev. E **47**, 3242 (1993).
[16] D. E. Wolf and J. Villain, Europhys. Lett. **13**, 389 (1990); S. Das Sarma and P. Tamborenea, Phys. Rev. Lett. **66**, 325 (1991); M. Siegert and M. Plischke, *ibid*. **68**, 2035 (1992); P. Smilauer and D. D. Vvedensky, Phys. Rev. B **48**, 17 603 (1993).
[17] M. Schroeder, M. Siegert, D. E. Wolf, J. D. Shore, and M. Plischke, Europhys. Lett. **24**, 563 (1993).
[18] J. W. Evans, D. E. Sanders, P. A. Thiel, and A. E. DePristo, Phys. Rev. B **41**, 5410 (1990); H. C. Kang and J. W. Evans, Surf. Sci. **271**, 321 (1992).
[19] J. Krug, M. Plischke, and M. Siegert, Phys. Rev. Lett. **70**, 3271 (1993).
[20] Y. L. He, H. N. Yang, T. M. Lu, and G. C. Wang, Phys. Rev. Lett. **69**, 3770 (1992).
[21] F. Family and T. Vicsek, *Dynamics of Fractal Surfaces* (World Scientific, Singapore, 1992).
[22] W. C. Elliott, P. F. Miceli, T. Tse, and P. W. Stephens (unpublished).
[23] J. G. Amar and F. Family, Surf. Sci. **365**, 177 (1996); in *Evolution of Epitaxial Structure and Morphology*, edited by A. Zangwill, R. Clarke, D. Jesson, and D. Chambliss, MRS Symposia Proceedings No. 399 (Materials Research Society, Pittsburgh, 1996), p. 95.
[24] For the bcc(100) surface the layer spacing is one-half the next-nearest-neighbor spacing in Fig. 1, while for the fcc(100) surface the relative vertical separation between successive layers (and therefore also the corresponding mound slope) is a factor of $\sqrt{2}$ times higher.
[25] S. C. Wang and G. Ehrlich, Phys. Rev. Lett. **75**, 2964 (1995); G. Ehrlich, Surf. Sci. **331–333**, 868 (1995).
[26] R. Stumpf and M. Scheffler, Phys. Rev. Lett. **72**, 254 (1994).
[27] This implies that, in the case of deposition with transient kinetics at a straight step edge, an additional downward hop is accepted with probability $\frac{1}{4}$.
[28] J. A. Stroscio, D. T. Pierce, and R. A. Dragoset, Phys. Rev. Lett. **70**, 3615 (1993).
[29] J. G. Amar and F. Family, Phys. Rev. Lett. **74**, 2066 (1995).
[30] J. G. Amar and F. Family, Phys. Rev. B **52**, 13 801 (1995).
[31] P. Smilauer and S. Harris, Phys. Rev. B **51**, 14 798 (1995).
[32] J. A. Stroscio (private communication).
[33] J. A. Meyer, J. Vrijmoeth, H. A. van der Vegt, E. Vlieg, and R. J. Behm, Phys. Rev. B **51**, 14 790 (1995).
[34] M. C. Bartelt and J. W. Evans, Phys. Rev. Lett. **75**, 4250 (1995).
[35] This result is based on the assumption, valid for m not too large, that there is at least one terrace between each step.
[36] S. F. Edwards and D. R. Wilkinson, Proc. R. Soc. London Ser. A **381**, 17 (1982).
[37] W. F. Egelhoff, Jr. and I. Jacob, Phys. Rev. Lett. **62**, 921 (1989).
[38] R. Kunkel, B. Poelsema, L. K. Verheij, and G. Comsa, Phys. Rev. Lett. **65**, 733 (1990).
[39] P. Smilauer and D. D. Vvedensky, Phys. Rev. B **52**, 14 263 (1995).
[40] M. Siegert and M. Plischke, Phys. Rev. E **53**, 307 (1996).
[41] I. M. Lifshitz and V. V. Slyozov, J. Phys. Chem. Solids **19**, 35 (1961); D. Huse, Phys. Rev. B **34**, 7845 (1986).
[42] L. Golubovic, in *Evolution of Epitaxial Structure and Morphology*, edited by A. Zangwill, R. Clarke, D. Jesson, and D. Chambliss, MRS Symposia Proceedings No. 399 (Materials Research Society, Pittsburgh, 1996), p. 251, and unpublished.
[43] E. Somfai and L. M. Sander (unpublished).